Isotacticity Effect on Crystallization and Melting in Poly(propylene) Fractions. 2. Linear Crystal Growth Rate and Morphology Study

James J. Janimak, Stephen Z. D. Cheng,* and Paul A. Giusti

Institute and Department of Polymer Science, College of Polymer Science and Polymer Engineering, The University of Akron, Akron, Ohio 44325-3909

Eric T. Hsieh

Research and Development, Phillips Petroleum Company, Bartlesville, Oklahoma 74004

Received July 2, 1990; Revised Manuscript Received November 6, 1990

ABSTRACT: Linear crystal growth rate and crystal morphology changes in a set of poly(propylene) (PP) fractions with similar molecular masses and distributions but different isotacticities have been studied via polarized light microscopy (PLM), transmission electron microscopy (TEM), and wide-angle X-ray diffraction (WAXD) methods. All but one of these PP fractions exhibit a regime III/II transition in their linear crystal growth rate data at a supercooling of about 48 K. At high supercoolings, two new crystal growth regions are observed for these PP fractions with low isotacticities. These crystallization regions are isotacticity dependent, which could be due to a disordered α-crystal form and cross-hatched branching. At a constant supercooling, the linear crystal growth rate data differ by about 3 orders of magnitude because of the isotacticity difference. Crystal morphology changes, in particular, the cross-hatching phenomenon, with crystallization conditions and isotacticity have been observed. At low crystallization temperatures the cross-hatched lamellae cannot be fully developed. Decreasing the isotacticity, on the other hand, reduces the cross-hatching density. Crystal growth behavior and its corresponding morphological changes are also discussed.

Introduction

Since 1958, when isotactic poly(propylene) (i-PP) became commercially available, the crystal growth behavior and morphology of i-PP have been extensively studied. The linear crystal growth behavior of i-PP data is usually obtained through polarized light microscopy (PLM). In 1984 Clark and Hoffman,[1] utilizing seven different data sources,[2-9] showed the existence of two crystal growth regimes. The occurrence of a regime III/II transition would exhibit a downward change in slope with increasing crystallization temperature or decreasing supercooling. The regime III to regime II transition occurred near 410.2 K, which corresponds to a supercooling of $\Delta T = 48$ K (an equilibrium melting temperature of 458.2 K was used). The experimentally observed ratio of slopes in plots of log $G + U^*/[2.303R(T - T_\infty)]$ vs $1/[T(\Delta T)f]$ at the regime III/II transition is 2.087, close to the theoretical value of 2. The fold surface free energy of $\sigma_e = 65$–70 erg/cm^2 led to a value for the work of chain folding of around 25 kJ/mol. Allen and Mandelkern reported a regime II/I transition at about 425.2 K, or $\Delta T = 56$ K (an equilibrium melting temperature of 481.2 K was used). They found that the regimes do not serve as boundaries between distinct morphological textures.[10] Recently, we have found that for low molecular mass i-PP fractions, the presence of a regime II/I transition is well-defined by both observations from linear crystal growth rate and overall crystallization measurements. For high molecular mass i-PP fractions, only the regime III/II transition can be found.[11,12]

Data from morphological observations, somewhat unique for the α-crystal form of i-PP (which crystallizes from both solution[13] and the melt[14-18]), show a three-dimensional array of a nearly orthogonal "cross-hatched" lamellar texture. Solution crystallization studies have elucidated the basic morphology as being lathlike chain-folded lamellar crystals. These crystals formed relatively open networks in solution-grown aggregates, while tightly interwoven textures appeared during melt crystallization. It has been observed that such lamellar branching is characterized by the constant angle between "daughter" and "mother" lamellae (80 or 100°). From the two almost orthogonal components of the cross-hatch, the radial R lamellae (mother lamellae) by themselves would generate negatively birefringent spherulites as in β-form spherulites. The tangential T lamellae (daughter lamellae) would generate their own positive birefringence. However, the latter occurs in combination with the R lamellae. The presence of the T lamellae reduces the negative birefringence and, if in sufficient quantity, may actually impart their own sign, rendering the spherulite positively birefringent. In fact, the type I and type II spherulites proposed by Padden and Keith[19] are distinguishable by the different degrees of cross-hatching. Without any cross-hatching the spherulite should be a type II. There appears to be no morphological distinct stage where the type I to type II transition occurs. Rather, it represents one stage in a continuously varying ratio of R and T lamellae in which the average birefringence becomes a compensating factor. The spherulite appears to be nonbirefringent when approximately one-third of its branches were estimated to be tangential.[20]

In our previous publication in this series,[21] we have demonstrated that for a set of PP fractions with similar molecular masses and molecular mass distributions but different isotacticities, a uniform inclusion model[22,23] can be applied to describe these crystals. This conclusion was supported by our wide-angle X-ray diffraction (WAXD), small-angle X-ray scattering (SAXS), and differential scanning calorimetry (DSC) measurements. In this paper, particular attention is served to the isotacticity and crystallization conditions and their influences on the kinetics and morphological change in these PP fractions.

* To whom correspondence should be addressed.

0024-9297/91/2224-2253$02.50/0

Table I
Molecular Characteristics and Thermal Properties of the PP Fractions

assignment	$M_w \times 10^{-3}$	M_w/M_n	isotacticity	T_m, K	ΔH_f, kJ/mol
PP(X-20)	202	2.6	0.988	457.0	8.68
PP(Y-17)	159	2.3	0.978	456.0	8.66
PP(Y-9)	189	3.0	0.953	453.4	8.61
PP(X-6)	209	1.8	0.882	446.2	8.47
PP(X-3)	190	1.6	0.787	436.2	8.28

Experimental Section

Materials and Samples. Five PP fractions were used, designated PP(X-20), PP(Y-17), PP(Y-9), PP(X-6), and PP(X-3), where the greater number (the constant enclosed in parentheses) represents a greater degree of isotacticity. These were labeled and provided by the Phillips Petroleum Co., Bartlesville, OK. Molecular characteristics such as molecular mass, polydispersity, isotacticity, and thermodynamic properties are summarized in Table I. On the basis of pentad sequences [mmmm] from high-resolution ^{13}C nuclear magnetic resonance (NMR) data, these PP fractions aligned predominantly in head-to-tail configurations. The isotactic component is randomly distributed along the chain. It is well-known that polymer crystallization behavior is a molecular mass dependent property. This dependence gradually diminishes when molecular mass exceeds 50 000. Therefore, the slight differences in molecular mass of these fractions (see Table I) are insensitive to the crystallization behavior except where there are different isotacticities.

To prepare the samples for PLM experiments, ~0.5-mg quantities of the PP samples were melted on a hot plate and inserted between two glass cover slips. The thickness of the polymer film was controlled to a thickness of 10 μm by an aluminum film wedge that was placed in between cover slips. The sandwiched specimens were then stored under vacuum at room temperature prior to their final heat treatment and measurement. For TEM and WAXD measurements, samples with a thickness of about 0.5 mm were crystallized from the melt in a temperature-controlled oil bath (Neslab TMV-40DD) with a precision of ±0.1 K under a dry nitrogen gas atmosphere.

Instrumentation and Experiments. A PLM (Nikon Labophot-pol) was used in conjunction with Mettler hot stages (FP-52). The specimens were heated to 20 K above their equilibrium melting temperatures on a hot stage and held there for 5 min to erase previous thermal history effects. The samples were then quickly shifted to another hot stage where a predetermined crystallization temperature, T_c, was maintained. After the hot stage reached thermal equilibrium, the crystal growth rates were measured during spherulitic or axialitic development. The linearity was ensured by successive measurements of the growth rate (different spherulite radii) at various time intervals prior to impingement effects. Five different trials at each temperature for each fraction were taken, and the standard deviation was better than ±4%. The crystallization time, t_c, was recorded with a chronograph timer. All measurements were performed under an atmosphere of dry nitrogen. The hot stage was calibrated with standard, sharp-melting substances around the temperature range of interest. Temperature control was better than ±0.2 K. The birefringence of the spherulite, Δn, is defined as $\Delta n = n_r - n_t$, where n_r and n_t are the refractive indices along the radial and tangential directions of the spherulites, respectively. These values were obtained on the PLM using an Ehringhaus compensator to measure path difference D. With knowledge of the sample thickness (h), therefore, one has $\Delta n = D/h$.

The α-form lamellar textures of melt-crystallized spherulites of the PP fractions have been studied by TEM following permanganate etching methods, developed by Bassett's group.[24,25] After the samples were crystallized for a predetermined time or completely crystallized, they were then quenched in liquid nitrogen. Bringing the samples back to room temperature led to further crystal perfection steps by a secondary crystallization process. However, the initial crystal morphology formed before quenching did not change very much. A standard two-stage replication technique was applied. A surface impression of the etched sample surface was obtained by using acetylcellulose film (Bioden R.F.A.) and a smear of acetone to wet the surface. This was followed by shadowing the samples with heavy metal (Au/Pd, 0.4/0.6) at an angle of 30° to the replica surface in a vacuum evaporator. Then a coating of spectroscopically pure carbon (200–500 Å thick) was applied perpendicular to the replica surface. The acetylcellulose film was dissolved away in acetone after the coating, leaving the coated replica intact. The replica was then picked up onto TEM grids (200 mesh). They were examined in the TEM mode of a JEOL JEM-T8 transmission electron microscope with 60-kV accelerating voltage.

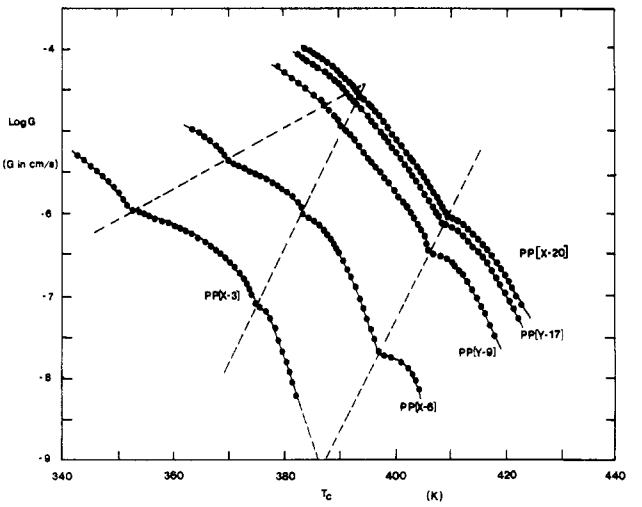

Figure 1. Relationships of logarithmic linear crystal growth rates with respect to crystallization temperatures for the PP fractions.

Wide-angle X-ray diffraction (WAXD) experiments were conducted through a Rigaku X-ray generator with a 12-kW rotating anode. A graphite crystal was used to monochromatize Cu Kα radiation. An angle range of 5–50° was scanned by the Rigaku powder diffractometer (D/Max-B) for these PP fractions after the samples were completely crystallized and quenched to room temperature. The d spacing was calibrated by using silicon powder (325 mesh size).

Results

Linear Crystal Growth Rates. The linear crystal growth rate behavior for these PP fractions is shown in Figure 1 as a function of crystallization temperature. The dashed lines demarcate regions of different crystal growth rate behavior. Two such boundaries are at constant supercoolings, $\Delta T = 48$ and 60 K, and the third supercooling boundary is isotacticity dependent. A change in the linear growth rate behavior with isotacticity at constant supercooling is apparent. For PP(X-20), PP(Y-17), PP(Y-9), and PP(X-6), the changes in the convex shapes of the crystal growth rate curves are at $\Delta T = 48$ K, indicative of the regime III/II transition (see below). However, for the PP(X-3) fraction ultraslow growth rates made it extremely difficult to observe experimentally. It is evident that for fractions of low isotacticity, the crystal growth is severely hampered. Nearly 3 orders of magnitude difference of the growth rates at a constant supercooling between fractions PP(X-20) and PP(X-3) is observed when the experimental data are compared in a supercooling region of ΔT = 50–60 K. At a supercooling of $\Delta T = 60$ K, the PP fractions underwent yet another change of the linear growth rate behavior similar to those observed at ΔT = 48 K. This change appears to be more evident for fractions of low isotacticity. Independent convex shape curves of the growth rate were very much apparent. This behavior is exemplified in the cases of PP(X-3) and PP(X-6). With increasing isotacticity, growth rate change becomes minor, as indicated in PP(X-20), PP(Y-17), and PP(Y-9), where

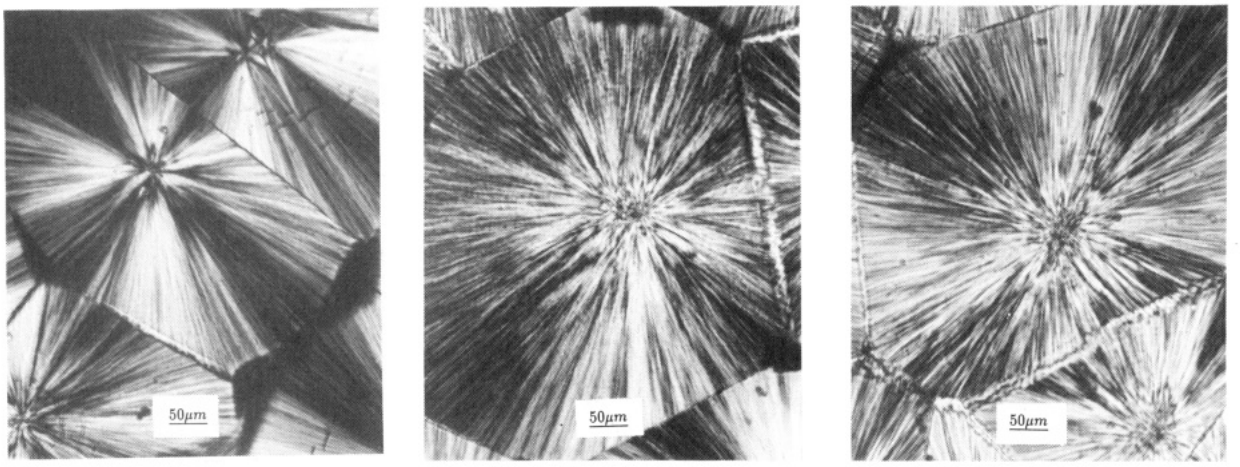

Figure 2. Crystal morphological change of PP(X-20) observed through PLM experiments at (a) 402.2 K (ΔT = 56 K), (b) 412.2 K (ΔT = 46 K), and (c) 422.2 K (ΔT = 36 K).

they are barely visible. This region can be regarded as an isotacticity-dependent "window".

Measurements of the linear crystal growth rates in excess of ΔT = 85 K for PP(X-3), 80 K for PP(X-6), 67 K for PP(Y-9), 65 K for PP(Y-17), and 64 K for PP(X-20) are not possible because of the increased primary nucleation density and/or crystal growth rate.

Crystal Morphologies As Observed by PLM. Focus here is on three PP fractions: PP(X-20), PP(Y-9), and PP(X-6), which are suitable candidates for describing the morphologies observed by PLM over an extensive isotacticity range. Observations via PLM have indicated subtle morphological differences that do not appear to correlate with the regime transitions. These morphological differences take the form of changes in the sign of birefringence, magnitude of the birefringence, and spherulite texture.

Figure 2a illustrates a typical spherulite crystalline morphology of PP(X-20) at T_c = 402.2 K or ΔT = 56 K crystallized from the melt. The classification of this type of spherulite, according to Padden and Keith's definition, is type I,[19] which is weakly positive (~0.0030) in birefringence. At higher isothermal crystallization temperatures for PP(X-20), the Maltese extinction cross pattern is still apparent. This is represented in (b) and (c) of Figure 2 at crystallization temperatures of T_c = 412.2 K or ΔT = 46 K and T_c = 422.2 K or ΔT = 36 K. The crystalline textures of Figure 2b,c are still spherulitic, but of a mixed type. The birefringence changes gradually to be weakly negative (~−0.0020). The overall appearance of PP(X-20) spherulites grown in these three different isothermal crystallization temperatures is an isotropic radiation type of growth. Rotating the polarizer and analyzer direction does not significantly change the extinction pattern and birefringence of the spherulites.

Similar morphological changes can be observed for PP(Y-9) crystallized at identical supercoolings as in the above PP(X-20) fraction. The isothermal crystallization temperatures were T_c = 397.4, 407.4, and 417.4 K, in descending order of supercooling, respectively. A highly impinged spherulitic texture with irregular extinction pattern (T_c = 397.4 K) is evident. With an increase in the crystallization temperature, the extinction cross pattern gradually becomes clearer. The texture at high crystallization temperature is relatively open and leaflike. An inherent reduction in primary nucleation is also observed. The birefringence changes from 0.0010 at ΔT = 56 K to −0.0025 at ΔT = 36 K.

Micrographs a–c of Figure 3 show morphologies of the PP(X-6) fraction grown at identical degrees of supercooling (as above). The isothermal crystallization temperatures were T_c = 390.2, 400.2, and 410.2 K, respectively. Figure 3a, crystallized at T_c = 390.2 K, represents irregular spherulitic textures arising from a high population of primary nuclei. The extinction cross pattern is not clear. Figure 3b shows spherulites (crystallized at 400.2 K) with a more or less regular extinction cross pattern. Figure 3c illustrates the texture grown at ΔT = 36 K and shows open and coarse spherulites, where each branch of the spherulite appears dendritic-like. The overall texture is close to two-dimensional. The birefringence changes from 0.0008 at ΔT = 56 K to −0.0030 at ΔT = 36 K.

Crystal Morphologies As Observed by TEM. TEM photographs for PP(X-20) crystallized at isothermal crystallization temperatures of 402.2, 412.2, and 422.2 K, just as in Figure 2a–c, are shown in Figure 4a–c. At this moment, the focus is only on the cross-hatched phenomenon. At low crystallization temperatures (Figure 4a), the population of high-density cross-hatched lamellae is quite predominant. The cross-hatched lamellae are small and underdeveloped. With increasing crystallization temperature (decreasing supercooling) to T_c = 412.2 K, these kinds of lamellae are clearly observed, as shown in Figure 4b. The cross-hatching density decreases, and, thus, both R and T lamellae are better developed. At the highest crystallization temperature of 422.2 K, the T lamellae are less apparent. The predominant morphology in Figure 4c is R lamellae. A similar observation was made for PP(Y-9) at T_c = 397.4, 407.4, and 417.4 K. It should be noted that at the lowest crystallization temperatures, for both fractions, the crystal growth behaviors are in the supercooling region between 48 and 60 K. The intermediate crystallization temperatures lead to the growth behavior of just above the supercooling boundary of 48 K. The highest ones are well above this boundary (see Figure 1).

On the other hand, for PP(X-6), the morphological change of the crystals at T_c = 375.2, 390.2, 400.2, and 410.2 K are observed. The lowest crystallization temperature (Figure 5a) is in the isotacticity "window" and no cross-hatched lamellae are observed. Figure 5b is in the supercooling region between 48 and 60 K. Interestingly

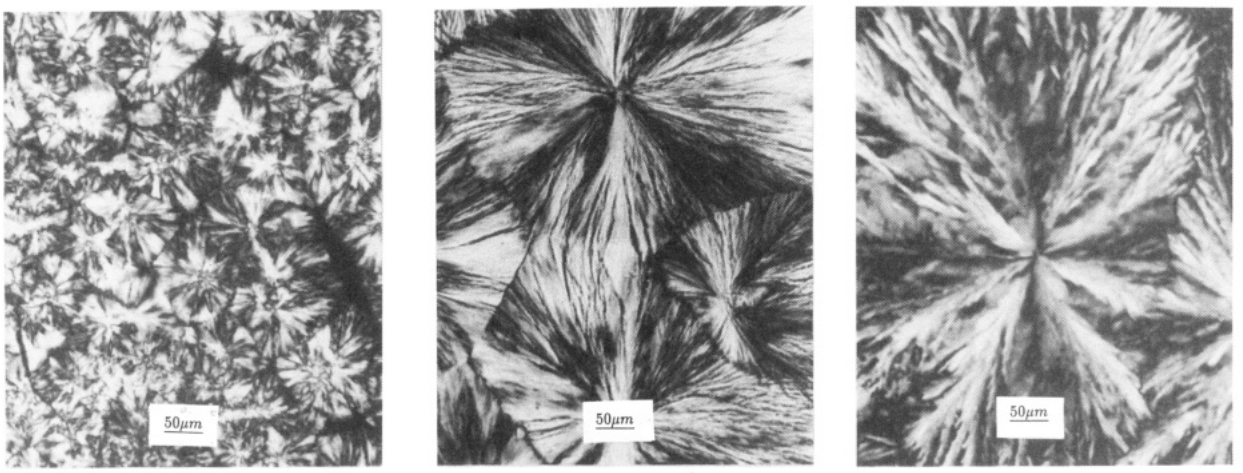

a $\Delta T = 56$ K b $\Delta T = 46$ K c $\Delta T = 36$ K

Figure 3. Crystal morphological change of PP(X-6) observed through PLM experiments at (a) 390.2 K (ΔT = 56 K), (b) 400.2 K (ΔT = 46 K), and (c) 410.2 K (ΔT = 36 K).

enough, the cross-hatching phenomenon comes back. When the crystallization temperature is further increased, the cross-hatched lamellae are still seen, but with a lower cross-hatching density. Comparing samples with high isotacticities at the same supercooling, the population of cross-hatched lamellae is drastically reduced.

Of special interest is the disappearance of the cross-hatched lamellae in the supercooling region of the isotacticity "window". To further confirm such observation, PP(X-3) was crystallized at T_c = 365.2 K (ΔT = 71 K). The absence of any cross-hatched lamellae is evident. A high crystallization temperature of 400.2 K (ΔT = 36 K) also yielded the absence of cross-hatched lamellae. This can be observed in Figure 6.

It is also surprising that at high crystallization temperatures the average lamellar thickness of the R lamellae is greater than that of the T lamellae, as long as the cross-hatching phenomenon is observed. At low temperatures, however, the difference between these two lamellar thicknesses is not apparent. Table II lists the lamellar thickness data observed through TEM for four PP fractions at different crystallization temperatures.

Crystal Structures As Observed by WAXD. Parts a and b of Figure 7 show the relationships between d spacings of crystallographic planes and crystallization temperatures for PP(X-6) and PP(X-3) fractions. Five independent runs at each temperature on WAXD were performed, with the deviations being represented by the error bars in the figures. Two particular crystallographic planes were studied, namely, the (110) and (040) planes. The d spacings of these planes decrease with increasing crystallization temperature. In particular, it is interesting to find that for both fractions the decrease of d spacings shows two steps, as exemplified in the figures. A steeper decrease has been seen at low temperatures, and a plateauing decrease at high temperatures. The changes in slopes for these two d spacings in Figures 7a and 7b occur at about 370 K for PP(X-6) and about 350 K for PP(X-3), respectively.

Discussion

The crystallization behavior and morphology of i-PP have been extensively studied in the past 30 years. Those pioneering works form the fundamental basis of our discussion. Focus here is on the isotacticity effect of two aspects: (1) Can we apply the regime theory[26-31] to describe our linear crystal growth data in these PP fractions? (2) Can we establish a correlation between the linear crystal growth behavior and morphological observations?

Following the present nucleation theory,[26-31] two regime transitions can be predicted. Over ten polymers have been reported to show such kinds of regime transitions as recently summarized by Hoffman and Miller.[32] In i-PP, as has been described in the introductory section, three regimes were found for low molecular mass i-PP fractions, and two regimes (regimes II and III) were observed in high molecular mass fractions.[1,10-12] For our PP fractions, the linear crystal growth rate data, shown in Figure 1, were also treated in the same way based on the nucleation theory, and the results are shown in Figure 8. Here, the equilibrium melting temperatures adopted are those listed in Table I, the glass transition temperature is 269.6 K, and $T_\infty = T_g - 30$ K. The "universal" constant for U^* of 6.28 kJ/mol is applied.[33] For PP(X-6) to PP(X-20), the regime III/II transitions were observed at ΔT = 48 K. For PP(X-3), this transition was anticipated based on the observed trends, but experimentally impossible due to extraordinary slow linear crystal growth rate (about 15 nm/day). At ΔT = 60 K, for both PP(X-6) and PP(X-3), a transition can be clearly identified with a decreased slope. However, this transition cannot be explained by current nucleation theory, since in the theory, regime III should be the last regime observed at low crystallization temperatures. On the other hand, for three PP fractions with higher isotacticities (≥0.95), this transition is not obvious. The identification of these transitions is actually on the boundary of experimental deviations. However, further decrease in crystallization temperature for both PP(X-3) and PP(X-6) leads to another upward transition. In particular, this transition does not occur at a constant supercooling as previous transitions do, but increases the transition temperatures with isotacticity. It is the so-called isotacticity "window" as described in the Results section.

Table III lists the kinetic data of crystal growth for the five PP fractions. It is evident that all the regime transitions showed ratios of the slopes between two neighboring regimes, occurring at ΔT = 48 K, whose values were in the vicinity of 2. This indicates that the transitions are regime III/II transitions, which can be described by

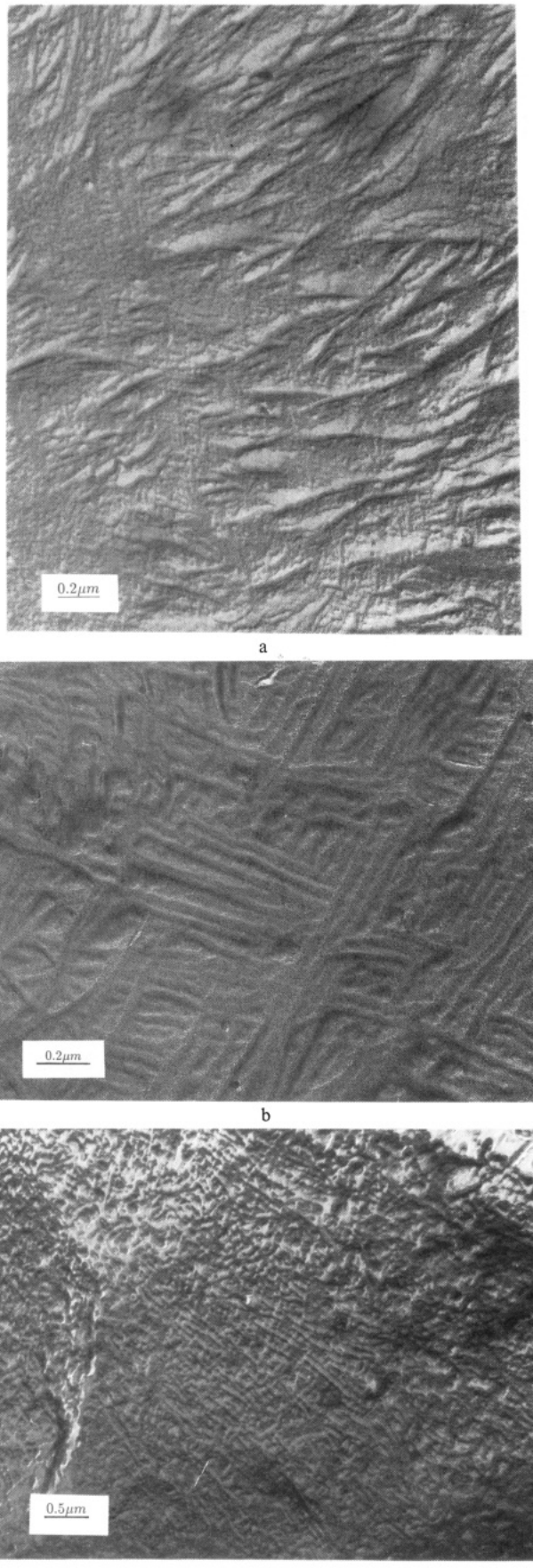

Figure 4. Crystal texture change of PP(X-20) observed through TEM experiments at (a) 402.2 K (ΔT = 56 K), (b) 412.2 K (ΔT = 46 K), and (c) 422.2 K (ΔT = 36 K).

nucleation theory.[26-31] From the slopes, one can calculate the products of lateral and fold surface free energies, $\sigma\sigma_e$, which are in the range of 700–1350 erg^2/cm^4 along the (110) growth plane. With decreasing isotacticity, the value of $\sigma\sigma_e$ increases, indicating an increase of roughness for both lateral and fold crystal surfaces. However, it is not possible to quantitatively distinguish the contributions to $\sigma\sigma_e$ from these two surfaces.

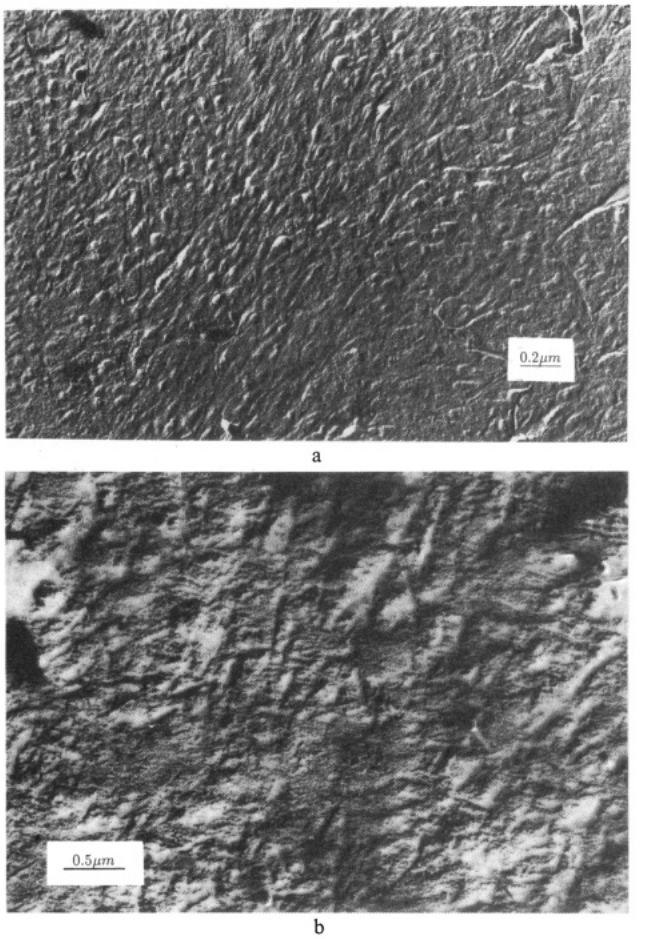

Figure 5. Crystal texture changes of PP(X-6) observed through TEM experiments at (a) 375.2 K (ΔT = 71 K) and (b) 390.2 K (ΔT = 56 K).

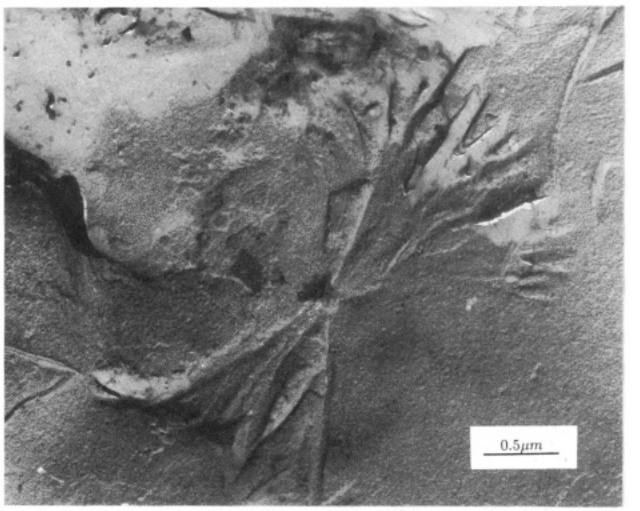

Figure 6. Crystal texture of PP(X-3) observed through TEM experiments at 400.2 K (ΔT = 36 K).

The observation of the isotacticity "window" is striking to us. The window seems to create two new regions if one still follows the nucleation theory.[26-31] The ratios between two neighboring slopes are surprisingly close to 2 (Table III). Our question is concerned with the cause of these

Table II
Lamellar Thicknesses of the PP Fractions at Different Supercoolings

assignment	supercooling (temp), K	R lamellar thickness, nm	T lamellar thickness, nm
PP(X-20)	36 (424.2)	40.3	30.4
	46 (412.2)	26.1	23.1
	56 (402.2)	22.0	~22.0
PP(Y-9)	36 (417.4)	46.2	33.0
	46 (407.4)	28.8	26.4
	56 (397.4)	25.1	~25.0
PP(X-6)	36 (410.2)	49.1	38.5
	46 (400.2)	38.5	29.2
	56 (390.2)	28.9	~28.0
	72 (375.2)	~21.0	
PP(X-3)	36 (400.2)	~57.7	
	71 (365.2)	~29.0	

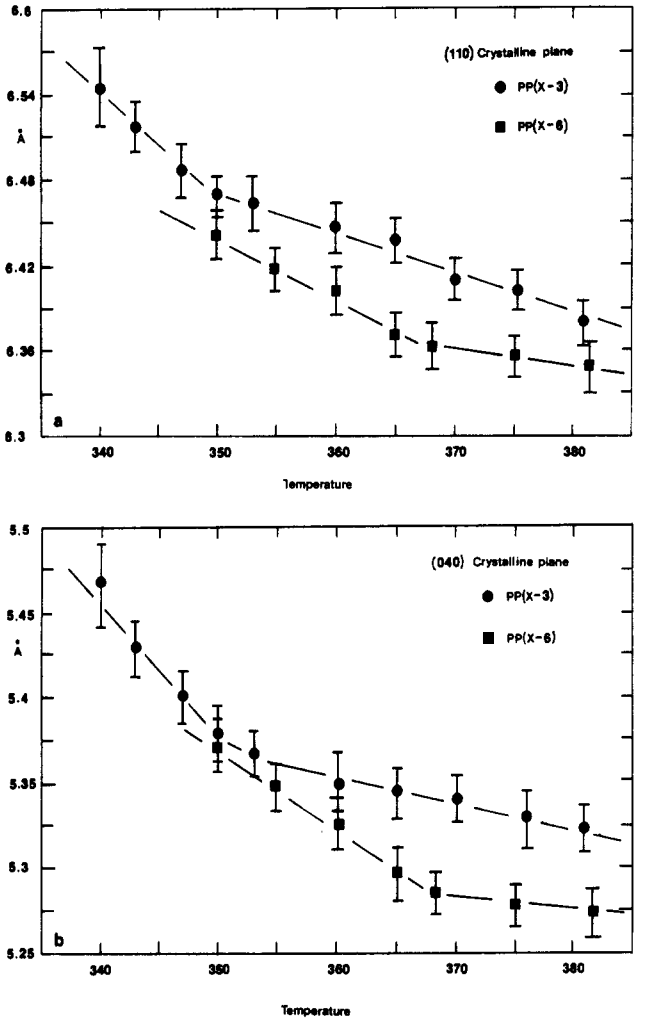

Figure 7. Relationships between d spacings of the crystallographic planes and crystallization temperatures (a) for the (110) plane and (b) for the (040) plane. The vertical lines are experimental error bars for five independent measurements per point.

kinds of new regions. From our WAXD experiments (Figure 7), it has been found that there are slope changes associated with decreases in d spacings (with temperature) for the PP fractions with low isotacticity contents [PP(X-6) and pp(X-3)]. These temperatures at which the observed change in the concave shapes of the crystal growth rate appears correspond well to the onset temperature of the isotacticity window [370 K for PP(X-6) and 350 K for PP(X-3)]. On the other hand, the cross-hatched lamellar texture cannot be observed for these PP fractions of low isotacticity content in the temperature regions where the

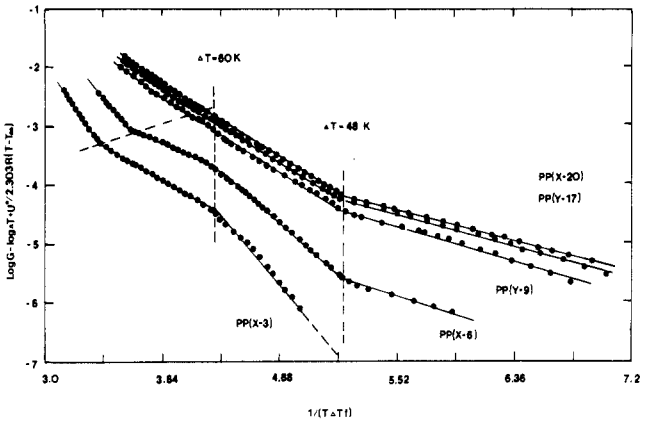

Figure 8. Relationships between $\log G - \log \Delta T + U^*/[2.303R(T - T_\infty)]$ and $1/[T(\Delta T)f]$ for these PP fractions.

Table III
Crystal Growth Kinetic Data Based on Nucleation Theory

assignment	$K_g \times 10^{-5}$,[a] K^2	$\sigma\sigma_e$, erg^2/cm^4	ratio
PP(X-20)	3.362 (III)	787	2.18
	1.543 (II)	722	
PP(Y-17)	3.431 (III)	796	2.07
	1.658 (II)	770	
PP(Y-9)	3.500 (III)	796	1.92
	1.819 (II)	827	
PP(X-6)	4.951	1051[b]	1.94
	2.556	1093	
	4.491 (III)	960	2.12
	2.119 (II)	906	
PP(X-3)	7.047	1342[b]	2.08
	3.385	1335	
	6.748 (III)	1314	

[a] Regime II and III growths are indicated in parentheses. They are assigned based on the work summarized in ref 1. [b] The calculations of $\sigma\sigma_e$ for PP(X-6) and PP(X-3) are based on b_0 = 4.40 Å and b_0 = 4.50 Å in the low-crystallization regions, respectively.

isotacticity windows appear, as has been observed through TEM. Our PLM results have shown that at such high supercoolings the crystalline textures are similar to those of low molecular mass i-PP fractions.[12] This indicates that the α-crystal form structure may be gradually disordered in the low-isotacticity PP fractions and consequently lead to the formation of the new regions as observed. It is certain that this disordering is isotacticity and temperature dependent. Unfortunately, the amount of change in molecular structure and crystal packing is not known. It may consist of larger degrees of irregularities in chain conformation and, therefore, defects within crystals. Further reduction in crystallization temperature leads to an even less ordered, smectic-like structure, as reported some years ago.[34-38] If we make the assumption of a distorted crystal lattice (disordered α-form), with a larger b_0 value, we obtain the calculated values of the product of surface free energies, $\sigma\sigma_e$, listed in Table III. They are higher than the values of $\sigma\sigma_e$ obtained through regimes II and III. This reveals that the crystals in those temperature regions are thermodynamically less stable when compared to the α-crystal form found at higher temperatures.

The changes of the crystal growth region at a supercooling of 60 K for both PP(X-6) and PP(X-3) are less understood. We speculate that they must be associated with the observed cross-hatching behavior. From our TEM observations, in the isotacticity windows there is almost no cross-hatched lamella to be observed, and beyond the windows the cross-hatching phenomenon comes back. This supercooling is perhaps a starting temperature where the cross-hatched lamellae are allowed to grow (see below).

One may speculate that the regime III/II transitions in these PP fractions are also attributed to diminishing cross-hatched lamellae. However, the disappearance of cross-hatched lamellae is a gradual process as we observed from TEM (Figures 4–6) and birefringence measurements. Furthermore, one must distinguish two different growths of the cross-hatched lamellae: the cross-hatched lamellae grown directly on the leading R lamellae; or those grown in between the leading lamellae. The former is close to the edges of the crystal growth front that is measured by PLM and usually observed at relatively low crystallization temperatures. This indicates that the R and T lamellae grow at almost the same time. Compact textures of spherulites grown at low temperatures do not generate enough space to fully develop the T lamellae. As a result, a high cross-hatching density with small T lamellae can be observed. Only relatively open textures may lead to well-developed T lamellae, as shown in Figure 4b. The latter is a delayed growth with the growth front of the R lamellae, as is usually seen at relatively high temperatures. As a consequence, the T and R lamellae show different thicknesses at high crystallization temperatures (Table II), possibly due to the short annealing time for the T lamellar and/or molecular segregation during the growth of R lamellae. Nevertheless, the temperature that indicates the change from the former to the latter cases does not correspond to the temperature of the regime III/II transition. The cross-hatched lamellae are depleted only at higher temperatures.

Of special interest is the isotacticity dependence of the cross-hatched lamellae in these PP fractions. On the basis of the TEM and birefringence observations, a clear tendency of decreasing cross-hatching density with isotacticity is observed. To explain this observation, one has to look in detail at the molecular mechanisms of the cross-hatching phenomenon. Three aspects—molecular, crystallographic, and morphological aspects of the cross-hatched lamellae—have been extensively discussed.[14-18,39-42] All the authors agree that there is an epitaxial growth involved. The most thorough study was recently made by Lotz and Wittmann.[18] They suggested that structurally in i-PP the T lamellae epitaxially grown occurs on the lateral (010) crystallographic plane of the R lamellae by a satisfactory interdigitation of the methyl groups of facing planes. This condition arises by the near identity of the sizes of the a and c crystallographic axes in the unit cell of the monoclinic α-form. From a molecular point of view, chains that deposit onto the (010) plane for the initiation of this epitaxy have the same helical handedness as chains in the (010) plane, but with a substantial angle (about 80 or 100°) in order to have favorable interactions of the methyl groups in the helices. This arrangement leads to a requirement of well-developed (010) crystallographic planes that can accommodate the deposition of a substantial chain length at near right angles to the substrate chain orientation.[18] In decreasing the isotacticity of these PP fractions, it is evident that the capability to retain such a regular (010) plane is reduced due to the configurational defects caused by random appearance of the methyl groups along the chain direction. As a consequence, the epitaxial nucleation process is increasingly hampered in decreasing the isotacticity. The cross-hatching density is thus reduced. We speculate that the depletion of cross-hatched lamellae at high crystallization temperatures may also be related to this epitaxial nucleation process. Nevertheless, this process is still some distance away from being fully understood. In particular, how does a chain deposit onto the (010) plane with a substantial chain length at a time? This type of crystallization criterion requires a fair degree of conformational regularity along the chain direction in the supercooled melt, which could lead to a significant departure from a random coil conformation.

Conclusion

This set of PP fractions has provided a unique opportunity to separate the isotacticity effect from other effects that may influence the linear crystal growth rates and crystal morphology changes. Several interesting observations have indicated the following: (1) There exists a regime III/II transition based on the current nucleation theory for these PP fractions with a range of isotacticity between 88.2 and 98.8%. The transition temperatures decrease with isotacticity but maintain a supercooling of 48 K from their equilibrium melting temperatures. (2) At low crystallization temperatures (the supercooling is larger than 60 K), two new crystal growth regions can be identified, which are isotacticity dependent (isotacticity windows). They are particularly prominent for these PP fractions with low isotacticities. Above ΔT = 60 K, two new crystallization regions are initiated, which are isotacticity dependent. A possible cause for such behavior may arise from a change of a regular α-crystal to a disordered α-crystal form. The boundary at ΔT = 60 K is possibly due to the introduction of cross-hatched lamellae. This phenomenon is absent when the isotacticity is higher than 95%. (3) With increasing crystallization temperatures, the cross-hatching density monotonically decreases for all these PP fractions. At low temperatures, the cross-hatched lamellae develop at almost the same time as the radial leading lamellae. The lamellar thicknesses are thus similar to each other. At high temperatures, however, the cross-hatched lamellae grow after the radial lamellae, and therefore, it shows a thinner lamellar thickness. (4) The cross-hatching density decreases with isotacticity, and, within the isotacticity window, very little cross-hatched lamellae can be found. This has been explained by the regularity of (010) crystallographic planes where epitaxial growths must be happening for the cross-hatched lamellae and, as such, is absent in the low isotacticity content PP fractions.

Acknowledgment. This work was supported by the Exxon Education Foundation.

References and Notes

(1) Clark, E. J.; Hoffman, J. D. *Macromolecules* **1984**, *17*, 878.
(2) von Falkai, B.; Stuart, H. A. *Kolloid Z.* **1959**, *162*, 138.
(3) von Falkai, B. *Makromol. Chem.* **1960**, *41*, 86.
(4) Binsbergen, F. L.; De Lange, B. G. M. *Polymer* **1970**, *11*, 309.
(5) Wlochowicz, A.; Eder, M. *Polymer* **1981**, *22*, 1285.
(6) Keith, H. D.; Padden, F. J., Jr. *J. Appl. Phys.* **1964**, *35*, 1286.
(7) Lovinger, A. J.; Chua, J. O.; Gryte, C. C. *J. Polym. Sci., Polym. Phys. Ed.* **1977**, *15*, 641.
(8) Goldfarb, L. *Makromol. Chem.* **1978**, *179*, 2297.
(9) Martuscelli, E.; Silvestre, C.; Abate, G. *Polymer* **1982**, *23*, 229.
(10) Allen, R. C.; Mandelkern, L. *Polym. Bull.* **1987**, *17*, 473.
(11) Cheng, S. Z. D.; Janimak, J. J.; Zhang, A.; Cheng, H. N. *Macromolecules* **1990**, *23*, 298.
(12) Janimak, J. J.; Cheng, S. Z. D. *Polym. Bull.* **1989**, *22*, 95.
(13) Khoury, F. J. *J. Res. Natl. Bur. Stand.* **1966**, *70A*, 29.
(14) Padden, F. J., Jr.; Keith, H. D. *J. Appl. Phys.* **1973**, *44*, 1217.
(15) Bassett, D. C.; Olley, R. H. *Polymer* **1984**, *25*, 935.
(16) Norton, D. R.; Keller, A. *Polymer* **1985**, *26*, 704.
(17) Lovinger, A. J. *J. Polym. Sci., Polym. Phys. Ed.* **1983**, *21*, 97.
(18) Lotz, B.; Wittmann, J. C. *J. Polym. Sci., Polym. Phys. Ed.* **1986**, *24*, 1541.
(19) Padden, F. J., Jr.; Keith, H. D. *J. Appl. Phys.* **1959**, *30*, 1479.

(20) Binsbergen, F. L.; De Lange, B. G. M. *Polymer* **1968**, *9*, 23.
(21) Cheng, S. Z. D.; Janimak, J. J.; Zhang, A.; Hsieh, E. T. *Polymer*, in press.
(22) Sanchez, I. C.; Eby, R. K. *J. Res. Natl. Bur. Stand.* **1973**, *77A*, 353.
(23) Sanchez, I. C.; Eby, R. K. *Macromolecules* **1975**, *8*, 639.
(24) Olley, R. H.; Hodge, A. M.; Bassett, D. C. *J. Polym. Sci., Polym. Phys. Ed.* **1979**, *17*, 627.
(25) Olley, R. H.; Bassett, D. C. *Polymer* **1982**, *23*, 1707.
(26) Lauritzen, J. I., Jr.; Hoffman, J. D. *J. Appl. Phys.* **1973**, *44*, 4340.
(27) Hoffman, J. D.; Frolen, L. J.; Ross, G. S.; Lauritzen, J. J., Jr. *J. Res. Natl. Bur. Stand.* **1975**, *79A*, 671.
(28) Frank, F. C. *J. Cryst. Growth* **1974**, *18*, 111.
(29) Hoffman, J. D. *Polymer* **1982**, *23*, 656.
(30) Hoffman, J. D. *Polymer* **1983**, *24*, 1.
(31) Hoffman, J. D.; Miller, R. L. *Macromolecules* **1988**, *21*, 3038.
(32) Hoffman, J. D.; Miller, R. L. *Macromolecules* **1989**, *22*, 3502.
(33) Hoffman, J. D.; Davis, G. T.; Lauritzen, J. I., Jr. In *Treatise on Solid-State Chemistry*; Hannay, N. B., Ed.; Plenum Press: New York, 1976; Vol. 3, Chapter 7.
(34) Natta, G.; Peraldo, M.; Corradini, P. *Rend. Accad. Naz. Lincei* **1959**, *24*, 14.
(35) Zannetti, R.; Celotti, G. C.; Fichera, A.; Francesconi, R. *Makromol. Chem.* **1969**, *128*, 137.
(36) Miller, R. L. *Polymer* **1960**, *1*, 135.
(37) Corradini, P. In *The Stereochemistry of Macromolecules*; Marcel Dekker: New York, 1968; Vol. 3.
(38) Fichera, A.; Zannetti, R. *Makromol. Chem.* **1975**, *176*, 1885.
(39) Geil, P. H. In *Polymer Single Crystals*; Interscience: New York, 1963, Chapters 3, 4.
(40) Selikhova, V. T.; Zubov, Yu. A.; Markova, G. S.; Kargin, V. A. *Polym. Sci. USSR (Engl. Transl.)* **1965**, *7*, 232.
(41) Padden, F. J., Jr.; Keith, H. D. *J. Appl. Phys.* **1966**, *37*, 4013.
(42) Morrow, D. R.; Newman, B. A. *J. Appl. Phys.* **1968**, *39*, 4944.